Characterization of Long Period Strong Ground Motion

M. Erdik[1], M.B. Demircioglu[2], K. Sesetyan[2], and E. Harmandar[2]

1. Prof., Bogaziçi University, Istanbul, Turkey
* Corresponding Author; email: erdik@boun.edu.tr
2. Dr., Bogaziçi University, Istanbul, Turkey

ABSTRACT

The performance-based earthquake engineering requires reliable assessment of long-period ground motion particularly for tall buildings, base-isolated structures, long bridges, and structures that are designed to deform beyond the elastic range. The important issues involved in such assessments are: Empirical and theoretical tools for prediction of displacement response spectra; Analysis and incorporation of near fault effects; Spectrum scaling for different damping ratios and; Time domain simulation of long-period ground motion. These issues are elaborated through (1) the principles for modification of design basis spectra in the long-period range; (2) guidelines for time domain simulation of long-period ground motions; and (3) rules for selecting and scaling ground motion records to address long-period effects. This paper aims to review and discuss these issues with developments on GMPRs for peak ground displacement and 10s spectral acceleration, and example applications on earthquake hazard assessment for 10s spectral accelerations and its deaggregation in the Marmara Region, Turkey.

Keywords:
Long-period ground motion; GMPE; Seismic hazard

1. Introduction

The philosophy of performance-based design has been widely accepted in recent years as a more rational approach in designing seismic resistant structures and the significance of the displacement response spectra has increased. Examples of structures with periods well beyond the spectral limits of acceleration or velocity sensitivity are long-span bridges (cable-stayed, suspension), high-rise buildings, isolated structures, and structures that are designed to deform beyond the elastic range. The recently adopted performance-based design approach requires that the expected peak ground displacements at long-periods are properly predicted. The accuracy of seismic design spectra given in current codes is not sufficient at these periods. There is also a need to develop guidelines to simulate or select ground motion records for such structures when performing nonlinear time-history analysis.

The state-of-the-art approach for site-specific assessment of the design basis ground motion dictates the deaggregation of the probabilistic hazard to yield the magnitude-distance-epsilon values that would contribute most to the hazard at the subject site. Although there are several physical models and the associated numerical techniques to simulate ground motions, they do not give consistent results, and their indiscriminate use does not necessarily yield reliable estimates of ground motions for design. The application of methods for earthquake-resistant design based on displacement demand is thus affected by the inaccurate definition of spectral response in the long-period range. The ability to determine motions at longer periods than before has an important application in displacement-based design. There is a strong need for the development of robust and reliable techniques for the assessment of long-period

earthquake ground motions especially for near field conditions. The efforts should address (1) the principles for modification of design basis spectra in the long-period range (2-10*s*); (2) guidelines for time domain simulation of long-period ground motions; and (3) rules for selecting and scaling ground motion records to address long-period effects.

2. Displacement Spectrum

Displacement spectra are a fundamental ingredient of displacement-based design procedures. Although some codes [e.g.1-2] define the displacement spectra, they are usually generated from the acceleration spectra assuming that the peak response under the assumption of steady state harmonic response. Such conversion of the acceleration spectra into displacement spectra results in unrealistic spectral shapes and displacement spectral ordinates [3-4]. The EC8 [2] response displacement spectrum shape is provided in Figure (1).

The essential features of this displacement spectrum are:

❖ The spectral displacement plateau (SD_{max} in Figure (1) starts at control periods T_D=1.2*s* for M<5.5 and T_D= 2*s* for M>5.5 (Note that the period T_D, as used in EC8 [2], will be denoted as T_C, to denote corner period, in the rest of this paper);

❖ The SD_{max} plateau extends up to control period T_E, dependent on soil conditions (T_E=4.5*s* for soil class A, T_E=5*s* for soil class B, T_E=6*s* for the other soil classes);

❖ The d_{max} plateau is reached at control period T_F=10*s*;

❖ The ratio of the maximum spectral displacement and the peak ground displacement is MSD/D_{max} = 2.5.
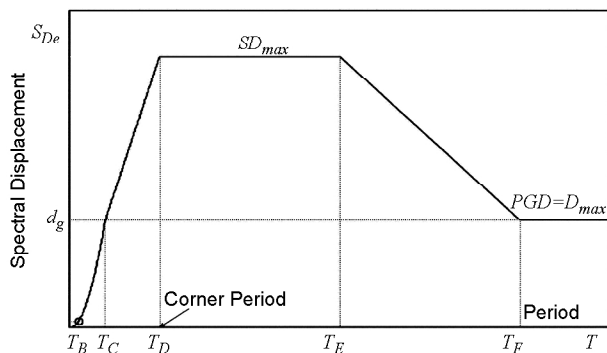

Figure 1. Elastic displacement spectrum [2].

The following, a relation between the peak ground displacement, D_{max} and the peak ground acceleration, A_{max}, is also in given EC8 [2] as:

$$D_{max} = 0.025 A_{max} S T_C T_D \qquad (1)$$

where, S is the soil amplification factor. S, and T_C depend on the magnitude (M<5.5 or M>5.5) and the soil class.

An important consideration in displacement spectra is the period at which the displacement response spectrum no longer increases. This period is known as the corner period T_C, see T_D in Figure (1).

The mean spectral displacement indicate an initial branch that increases up to a corner period (varying from few seconds to about 8*s*, increasing with magnitude), followed by a second branch that asymptotically approaches the *PGD*. At long-periods (10*s* and above), the displacement spectra scales linearly with magnitude.

Concern has been expressed that the EC8 spectral ordinates may be excessively low at longer periods, particularly if compared with those defined in IBC [1], where the constant displacement plateau commences at the corner periods ranging from 4 to 16*s*, whereas the EC8 Type 1 spectrum has a corner period equal to only 2*s*.

In general the corner period needs to be calculated either on the basis of empirical data or seismic source scaling models. In this respect the following relationships between the corner period and the moment magnitude (M_w) has been proposed for the United States [5].

$$log\ T_D = -1.25 + 0.3\,M_w \qquad (2)$$

2.1. Predictive Equations for Spectral Displacement

Bommer and Elnashai [4], Faccioli et al [6], Akkar and Bommer [7] and Cauzzi et al [8] have developed empirical relationships for the prediction of spectral displacement amplitudes on the basis of available strong motion data. Figure (2) provides *DRS* for rock sites for different moment magnitudes, focal distance and damping ratio.

2.2. Damping Scaling (Spectral Reduction Factors)

In seismic design codes, the spectra for damping levels higher than 5% are obtained by applying scaling factors (η) to the ordinates of the 5% damped spectrum, see Figure (3). The following expressions
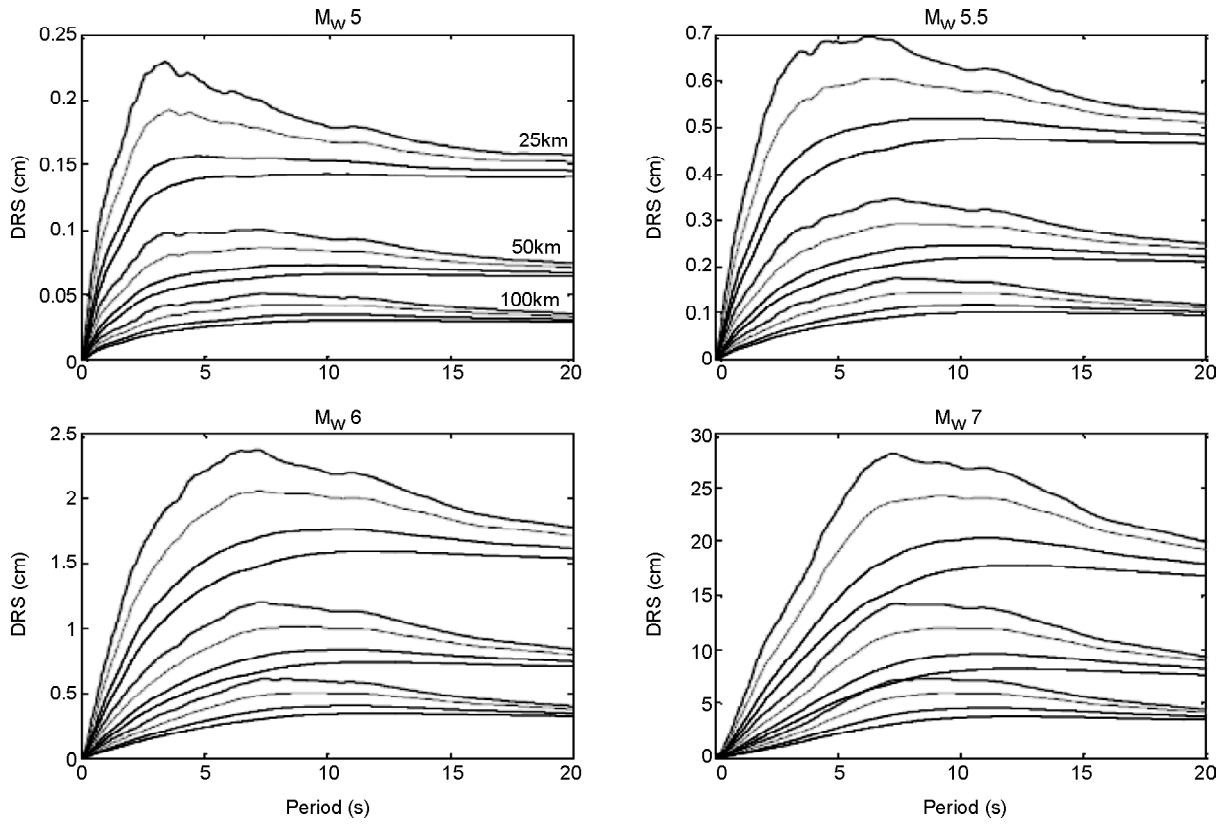
Figure 2. Displacement spectra for rock sites for different moment magnitudes, focal distance and damping ratio [8].
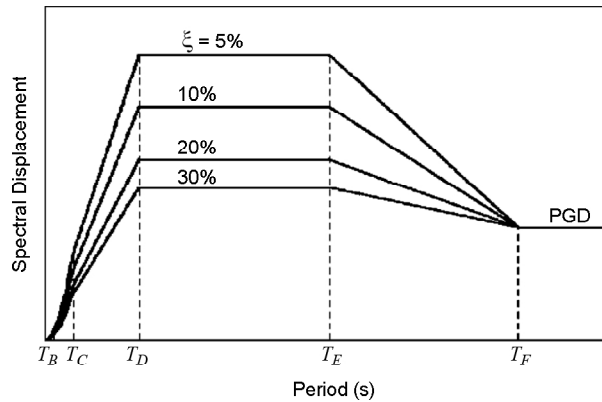

Figure 3. EC8 displacement spectra for different damping ratios.

for relating the displacement response spectra for a damping ratio of ξ to the elastic spectrum for $\xi = 0.05$ was presented respectively in [2] and [9] as:

$$\eta = \sqrt{\frac{0.07}{0.02 + \xi}} \qquad (3)$$

$$\eta = \sqrt{\frac{0.10}{0.05 + \xi}} \qquad (4)$$

Priestley et al [10] claims that Eq. (3) [9] provides a better representation of the damped spectra.

For near-source directivity effects Priestley et al [10] and Priestley [11] has proposed the following modification of the EC8 spectral scaling factor in Eq. (5) for the forward directivity velocity pulse:

$$\eta = \left(\frac{0.07}{0.02 + \xi}\right)^{0.25} \qquad (5)$$

3. Prediction of Peak Ground Displacement (PGD)

3.1. Empirical Attenuation Relationships

The use of the proposed analytical expressions

for the displacement spectra requires that the peak ground displacement d_{max} be properly predicted. Existing attenuation relationships for d_{maK}, see Gregor and Bolt [12], for California data; Bommer et al [13] and Tromans and Bommer [14], for European data, are mainly based on analog records and suffer from the well-known instrumental limitations and long-period noise at periods larger than about 3s.

Using essentially the same dataset used for the derivation of the spectral acceleration attenuation relationships in Europe by Ambraseys et al [15], Bommer et al [13] derived the following attenuation model for the *PGD* (in *cm*) valid for periods under 3s.

$$log(PGD) = -1.757 + 0.526 M_s - \quad (6)$$
$$1.135 log(r) + 0.114 S_a + 0.217 S_S$$

where S_a is a binary variable taking a value of 1 for stiff soil sites and 0 otherwise and S_S being similarly defined for soft soil sites. The site classification scheme is based on the average shear wave velocity, V_{s30}, over the upper $30m$ at the site. The sites are those with V_{s30} values greater than $750m/s$, soft sites those with V_{s30} less than $360m/s$ and stiff soil sites are those with intermediate values. The term r is defined by:

$$r = (d^2 + 10.24)^{0.5} \quad (7)$$

where d is the shortest distance from the surface projection of the fault rupture in km. Bommer et al [13] reports that the values of *PGD* predicted by the Eq. (6) are comparable to those predicted by the relationships of Gregor and Bolt [12].

Gregor et al [16] has provided *PGV* and *PGD* attenuation relationships based on regression results from two datasets of strong ground motion parameters. The first dataset is referred to as "dynamic" and consists of the *PEER* processed recorded strong ground motions from earthquakes that have occurred in active tectonic regions. This dataset includes the 1999 Kocaeli Turkey (*M*=7.4), the 1999 Chi-Chi Taiwan (*M*=7.6), and the 1999 Duzce Turkey (*M*=7.1) earthquakes. The second dataset is termed "static" and is similar to the first but with the near source (i.e., rupture distances less than $20km$) strong ground motion time histories processed using a method designed to preserve the recorded static displacements. These two datasets have a range in

magnitude of *M* 4.4 to *M* 7.6 and span a distance range of $0.1km$ to $267.3km$.

For the regression analysis, each recording site was classified as either "soil" or "rock" site conditions. The "rock" classification includes those sites that are located on shallow stiff soil deposits and the "soil" classification includes those strong ground motion sites which are located on both deep broad and deep narrow soil deposits.

The model (Model *D* of Gregor et al [16]) is defined as,

$$In(GM) = \theta_1 + \theta_2 M + (\theta_2 + \theta_3) In(D + e^{\theta_s}) +$$
$$\theta_6 (1 - S) + \theta_7 (M - 6)^2 +$$
$$\theta_8 F + \frac{\theta_8}{tanh(D + \theta_{10})} \quad (8)$$

where *GM* is the peak ground motion parameter (*PGA*, *PGV*, *PGD*), *S* is the site condition term and is equal to 1 for rock sites and 0 for soil sites, *M* is the earthquake magnitude, *F* is the mechanism term and is equal to 0.0 for strike-slip, 0.5 for reverse/oblique and unknown, and 1.0 for thrust mechanisms, and *D* is the rupture distance.

A new *PGD* attenuation relationship is derived using the updated database of the *PEER* strong motion database for the *NGA* Project. This dataset has a range in magnitude of $M_w = 4.27$ to $M_w = 7.9$ and span a distance range of $0.44km$ to $557.63km$. *PGD* values are the geometric average of the two orthogonal horizontal components orientated randomly. The distribution of records in magnitude-distance is shown in Figure (4a). The derivation of the model is explained in the following section. The functional form is defined as,

$$PGD = 3.275 \left(\frac{1}{r} \right) 10^{(M-5)} \quad (9)$$

where *PGD* is peak ground displacement in cm; r is the epicentral distance in *km*, and *M* is the earthquake magnitude.

The residuals between the observed *PGD* values and the predicted *PGD* values computed by the new relation, with respect to distance are shown in Figure (4b).

The predicted median *PGD* values from the new relation are compared with observed *PGD* values in Figure (5), and with those of Gregor et al [16], Cauzzi et al [8], and Campbell and Bozorgnia [17] in Figure (6).
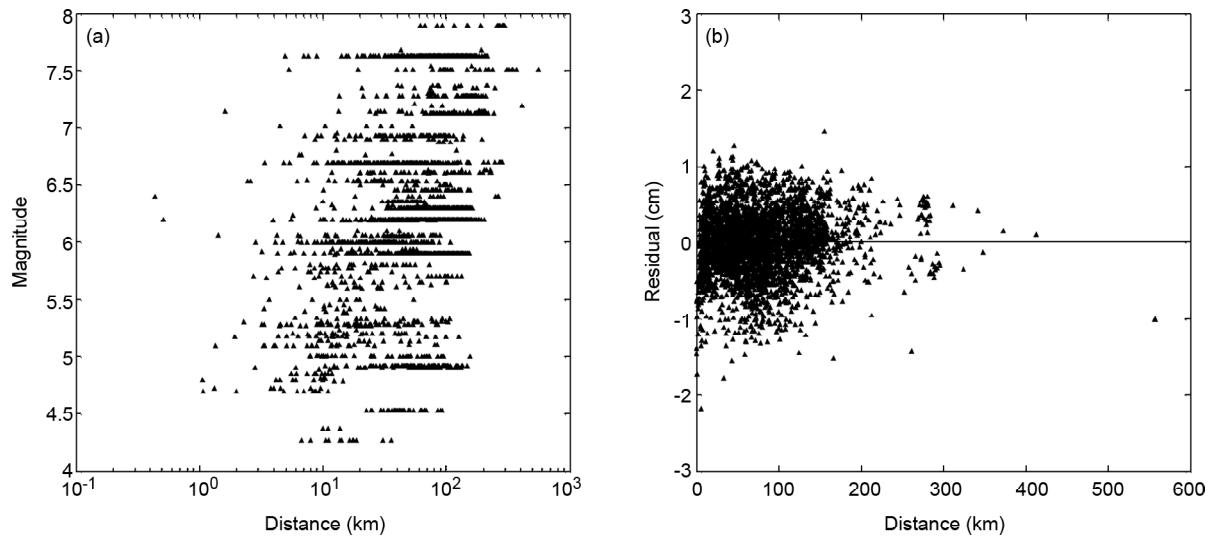
Figure 4. (a) Distribution of the dataset with respect to magnitude and distance, (b) the residuals and distance.
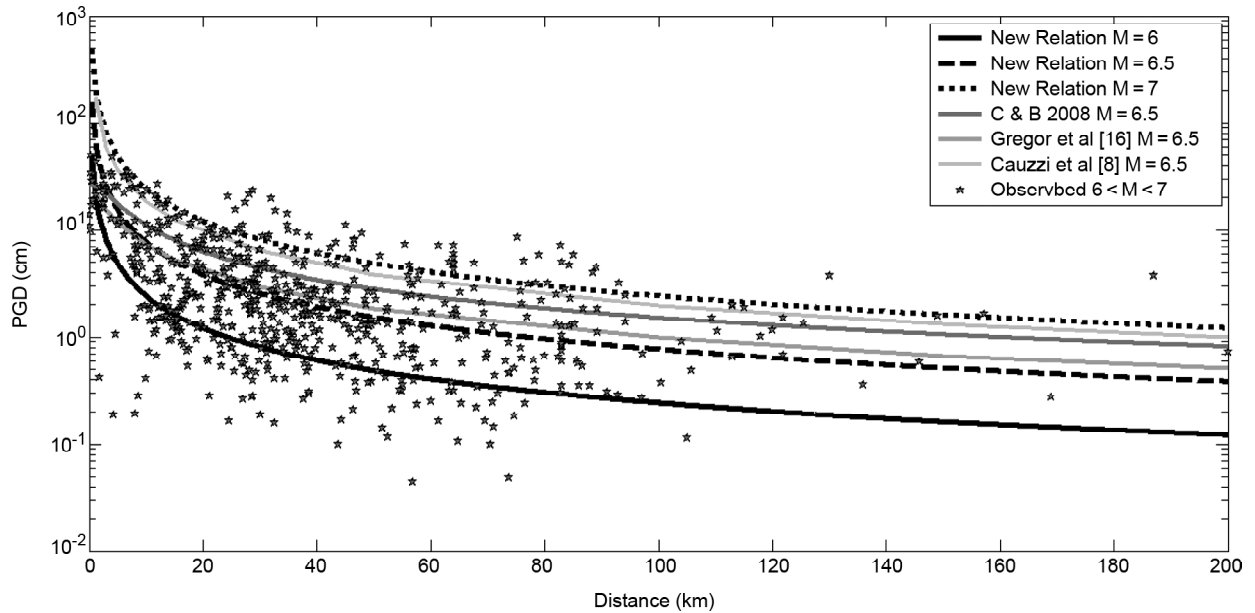

Figure 5. The predicted median PGD values from the new relation are compared with observed PGD values.
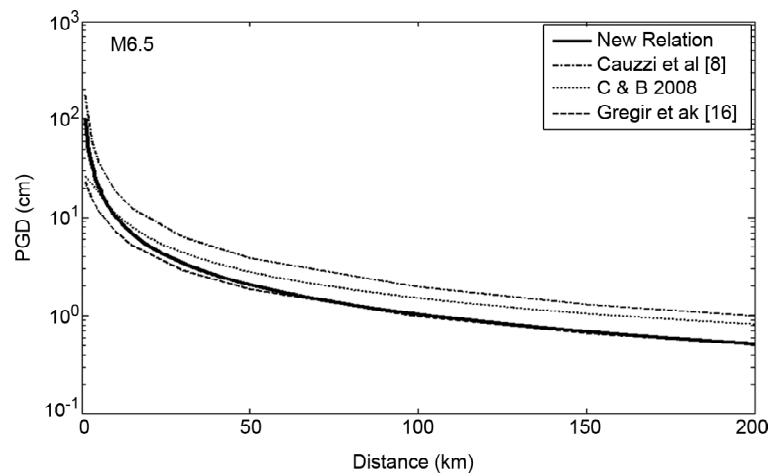

Figure 6. Comparison of proposed ground motion prediction equation with Gregor et al [16], Cauzzi et al [8], and Campbell and Bozorgnia [17].

3.2. Analytical Attenuation Relationships

On the basis of the work by Faccioli et al [6], Priestley et al [10] suggests that the corner period and the displacement amplitude (SD_{max} in mm) for 5% damping be given by the following relationships:

$$T_C = 1.0 + 2.5 (M_W - 5.7) \tag{10}$$

$$SD_{max} = C_S \frac{1}{r} 10(M_W - 3.2) \tag{11}$$

where r is the epicentral distance in km, and C_S is the site factor ($C_S = 1.0$ for firm ground).

Cauzzi et al [8] suggest that SD_{max} level can be simply defined by the spectral displacement at $10s$ (SD ($10s$)).

A theoretical attenuation relation for the far field maximum ground displacement is derived by Faccioli et al [6] from the Brune model,

$$log_{10}(d_{max}) = -4.46 + 0.33 \, log(\Delta\sigma) + M - log(R) \tag{12}$$

where $d_{max}(cm)$ is the maximum ground displacement, $\Delta\sigma(MPa)$ the stress drop and $R(km)$ the focal distance.

For field displacement from a point shear dislocation in a homogenous half space [18-19].

$$u(r,t) = \frac{R^{\theta\varphi}}{4\pi\rho\beta^3 r} \frac{M_0}{\tau} \left[\frac{t - \left(r/\beta \right)}{\tau} \right] e^{-\frac{1}{\tau}\left[t - \left(\frac{r}{\beta} \right) \right]} \tag{13}$$

where

$u(r, t)$: is the shearwave displacement at distance r from the shear dislocation.

$R^{\theta\phi}$: is the angular radiation pattern

ρ: is mass density of the medium.

μ: is the shear modulus of rigidity of the medium.

τ: is the characteristic rise parameter (time) controlling the rate of dislocation, $\tau = 1/w_c$ where w_c is the corner frequency

β: is the shear wave propagation velocity

M_0: is the seismic moment, $M_0 = \mu A u_T$, where A is the total rupture area and u_T is the total displacement at the source reached at the rise time, T

Beresnev [20] has shown that under certain assumptions

$$w_c = \frac{1}{\tau} \cong \frac{1}{T} \quad ve \quad T \cong 1.68 \tag{14}$$

The rise time T can also be related to source radius $D/2$ through the rupture velocity V_R by (as-

suming rupture starts at the central and propagates outward).

$$T = \frac{(D/2)}{V_R} \tag{15}$$

If we assume that $V_R = 0.8\beta$.

$$\tau \cong 0.74 \frac{(D/2)}{\beta} \tag{16}$$

$$M_0 = \mu A u_T \tag{17}$$

Assuming that the average shear strain over the dislocation can be given as $u_T/(D/2)$, the change in shear stress $\Delta\sigma$ (stress drop) can be expressed as:

$$\Delta\sigma = \mu \frac{u_T}{D/2} \tag{18}$$

and assuming circular dislocation $A = \pi \left(\frac{D}{2} \right)^2$

$$M_o \cong \Delta\sigma\pi \left(\frac{D}{2} \right)^3 \quad and \quad \left(\frac{D}{2} \right) \cong \left(\frac{M_o}{\pi\Delta\sigma} \right)^{1/3} \tag{19}$$

Using Eq. (16) and $M_0 = \Delta\sigma (D/2) A$

$$\tau \cong 0.5 \frac{\left(M_0/\Delta\sigma \right)^{1/3}}{\beta} \tag{20}$$

Through taking the derivative of Eq. (13) with respect to t and setting it to zero, it can be shown that the maximum value of $u(r, t)$ (for given r) is reached at $\tau = t - \frac{r}{\beta}$ and is given by

$$D_{max} = U_{max}(r) = \frac{R^{\theta\varphi}}{4\pi\rho\beta^3} \frac{1}{r} \frac{1}{e} \frac{1}{\tau} M_0 \leq u_T \tag{21}$$

where "e" is the base of the natural logarithm.

Substituting Eq. (20) into Eq. (21):

$$D_{max}(r) = \frac{R^{\theta\varphi}}{4\pi\rho\beta^3 e} \frac{1}{0.5(1/\Delta\sigma)^{1/3}} \frac{M_o^{2/3}}{r} \leq u_T \tag{22}$$

As such, the peak ground displacement has the following proportionalities:

$$D_{max}(r) \propto (1/r)(\Delta\sigma)^{1/3} M_o^{2/3} \tag{23}$$

Similar results have also been developed by Faccioli et al [6].

Relying on the assumptions commonly used in seismology ($R^{\theta\varphi} = 0.78$, $\beta = 3800 m/s$; $\rho = 2800 kg/m^3$; $e = 2.7$) and, noting that the stress drop generally varies between 10 and 100bar, $\Delta\sigma = 10\text{-}100 bar = 1\text{-}10 MPa$ [21]. It can be shown that

$$D_{max}(r) = (1.2/r)10^{-10} M_o^{2/3} \quad \text{(for } \Delta\sigma = 1 MPa) \quad (24)$$

$$D_{max}(r) = (2.5/r)10^{-10} M_o^{2/3} \quad \text{(for } \Delta\sigma = 10 MPa) \quad (25)$$

where D_{max} is m, M_o is in Nm and r is in m.

Using the definition of M_w

$$M_0 = 10^{1.5 M_w + 9.05} \quad (26)$$

And treating r in $km's$

$$D_{max} = (1.2/r)10^{M_w - 7} \quad \text{(for } \Delta\sigma = 1 Mpa) \quad (27)$$

$$D_{max} = (2.5/r)10^{M_w - 7} \quad \text{(for } \Delta\sigma = 10 Mpa) \quad (28)$$

Erdik and Durukal [19] provides the following relationships for the corner frequency ($f_c = \frac{1}{\omega_c}$) and the peak ground displacement $PGD = D_{max}$:

$$\log f_c \cong 6.2 - \frac{1}{3}(1.5 M_w + 9.05) = 3.2 - 0.5 M_w$$

or $\qquad\qquad\qquad\qquad\qquad\qquad\qquad (29)$

$$f_c \cong 10^{(3.2 - 0.5 M_w)}$$

where $\Delta\sigma$ is the stress drop. Please note that to obtain SD_{max} from D_{max} a factor of 2.5 needs to be applied to the D_{max}.

4. Simplified Displacement Response Spectra

Priestley et al [10] suggests the general idealized displacement spectra shape as illustrated in Figure (7). Apart from an initial period range up to about 0.5s, the displacement spectra is considered to increase linearly with period up to a period T_C,
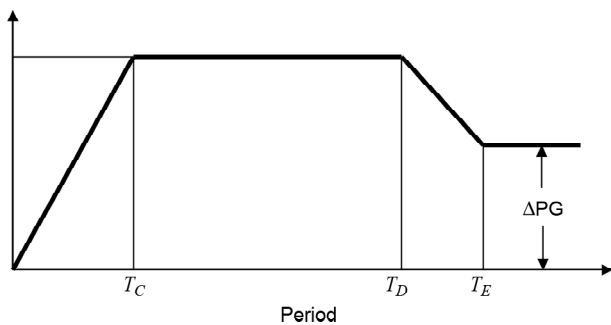
termed the comer period, with a subsequent plateau of displacement up to a period T_D, followed by a decrease in displacement up to a period T_E, at which stage the response displacement has decreased to the peak-ground displacement (*PGD*). Information on the period at which the response displacement starts to decrease is less reliable and is of little interest to the designer of other than extremely long-period structures (such as very long suspension bridges and large-diameter fluid storage tanks, where the sloshing periods may be very long).

On the basis of the work by Faccioli et al [6], Priestley et al [10] suggests that the displacement response spectra could be reasonably represented as linear up to a displacement plateau initiating at a corner period, T_C (in s), the value of which depends on the moment magnitude, M_w:

$$T_D = 1.0 + 2.5(M_W - 5.7) \quad (30)$$

with a corresponding displacement amplitude (D_{max} in mm) for 5% damping of

$$D_{max} = C_S \frac{1}{r} 10^{(M_w - 3.2)} \quad (31)$$

where r is the epicentral distance (or nearest distance to the fault plane for large earthquakes) in km, and where C_S is the site factor ($C_S = 1.0$ for firm ground, $C_S = 0.7$ for rock, $C_S = 1.4$ for intermediate soil, $C_S = 1.8$ for very soft soil).

Cauzzi et al [8] suggest the following simple approximate bilinear shape for the 5% displacement response spectrum, see Figure (8).

The 5% *DRS* defined as:

$$DRS(T) = \frac{D_{10} F(T; V_{S30})\eta}{T_D} T \quad 0 < T < T_D \quad (32)$$

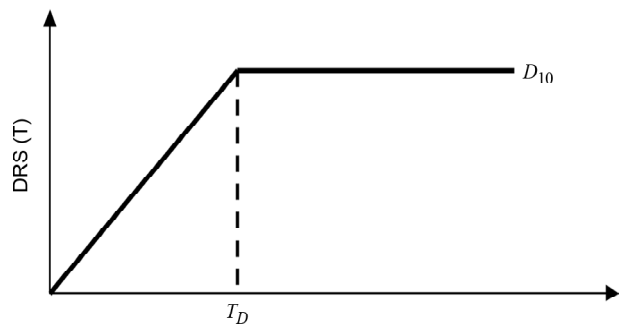$$DRS(T) = D_{10} F(T; V_{S30})\eta \quad T > T_D \quad (33)$$

Figure 7. General characteristics of elastic displacement response spectra.

Figure 8. Approximation to elastic displacement response spectra [8].

D_{10} is the spectral value corresponding to the constant long-period branch of the *DRS*, while T_D is the corner period, to be computed as

$$T_D = \frac{2\pi D_{10}}{(PSV)_{max}} \qquad (34)$$

where $(PSV)_{max}$ is the maximum value of the pseudo-velocity response spectrum and the term $F(T; V_{S30})$ is the spectral amplification factor due to local site conditions (equal to 1 for ground type *A* sites).

5. Long-Period Ground motion Pulses

Near-fault ground motions often contain long-period pulses and permanent ground displacements caused by rupture directivity effects. For large magnitude earthquakes, the directivity effects are generally associated with long-period (about 2-3*s*) ground motions consisting predominantly of horizontally polarized *SH*-waves with a *PGV* in the vicinity of 1*m/s*. For sites located close to faults, the strike-normal spectral amplitude is larger than that of the strike-parallel at periods longer than 0.6*s* in a manner that depends on magnitude, distance, and azimuth [22]. Since the near fault ground motions are characterized by a relatively simple long-period pulse of strong motion, rather than by a

stochastic process having relatively long duration that characterizes more distant ground motion, there is a growing understanding that the response spectrum alone is not capable of adequately describing the seismic demands presented by a near-fault pulse. As such, the ground motion input may need to be a time history instead of a response spectrum to adequately characterize the near-fault ground motions. The near fault ground motions containing forward rupture directivity effects may be simple enough to be represented by time domain pulses, thus simplifying the specification of ground motion time histories for use in structural response analyses.

The time domain parameters that describe the near-fault pulse (for forward rupture directivity conditions in the fault-normal direction) are its period, amplitude and number of half-cycles. The response spectrum that would result from a half-cycle displacement pulse was first investigated by Veletsos and Newmark [23] as illustrated in Figure (9).

Faccioli et al [6] have derived analytical expressions for the long-period displacement spectrum corresponding to different ground-motion pulse shapes. An example of a fling-step pulse that can be produced by a large magnitude earthquake (*Mw>*
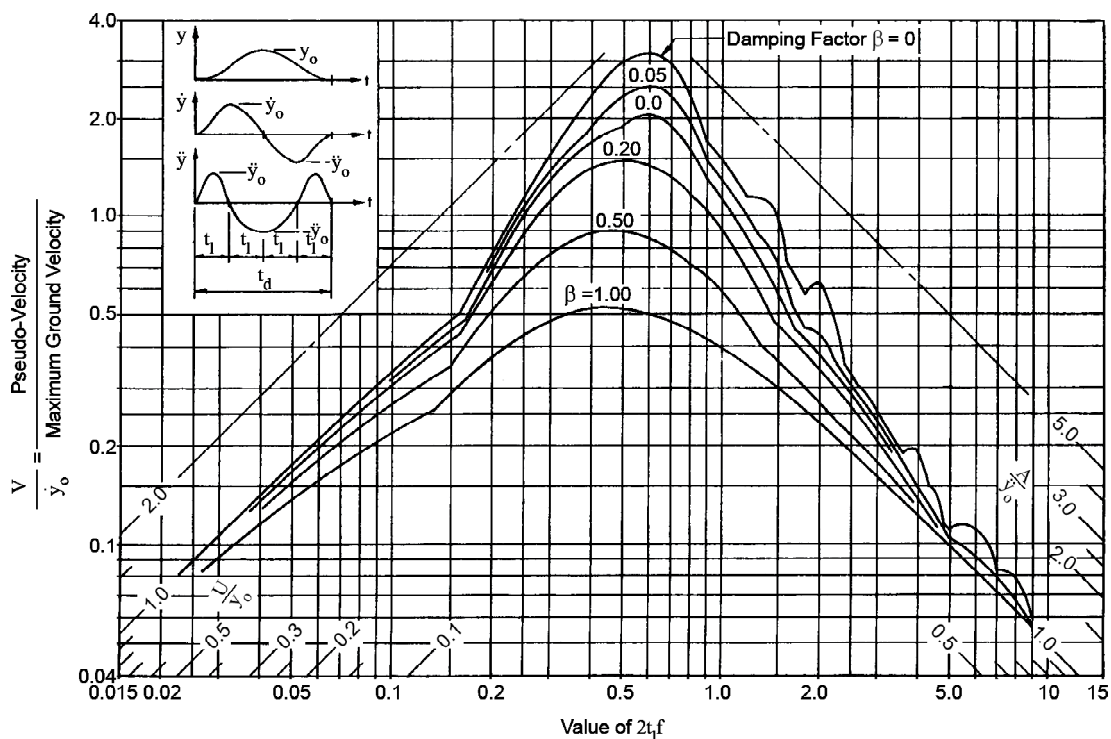

Figure 9. Response spectra for a half cycle displacement pulse [23].

7.5) and the corresponding normalized displacement spectra is provided in Figure (10). Faccioli et al [6] reports that the displacement spectrum can be approximated by simple displacement pulses, defined by the period $2t_0$ and the peak value d_{max}. The basic features of the displacement spectrum at long-periods are quite realistic since the dependence is on the shape of the displacement pulse rather than the acceleration.

A variety of researchers have assembled sets of pulselike or near-fault ground motions [e.g. 24-27]. Most of these methods use nonlinear optimization to fit a truncated sine wave to the pulse. Baker [28] developed a method for quantitative identifications of ground motions containing strong velocity pulses, such as those caused by near-fault directivity.

The approach uses wavelet analysis to extract the largest velocity pulse (amplitude ands period) from a given ground motion.

Somerville [29] has obtained the following relationships for the near-fault, fault-normal forward directivity pulse period (T) and the peak velocity (PGV) in terms of moment magnitude Mw and closest distance:

$$\log T = -3.1 + 0.5 M_W \tag{35}$$

$$\log_{10} PGV = -1.0 + 0.5 M_W - 0.5 \log_{10} R \tag{36}$$

The velocity and acceleration pulses (one period) that would result from the application of Eqs. (35) and (36) and the corresponding acceleration spectra are provided in Figures (11) to (13).
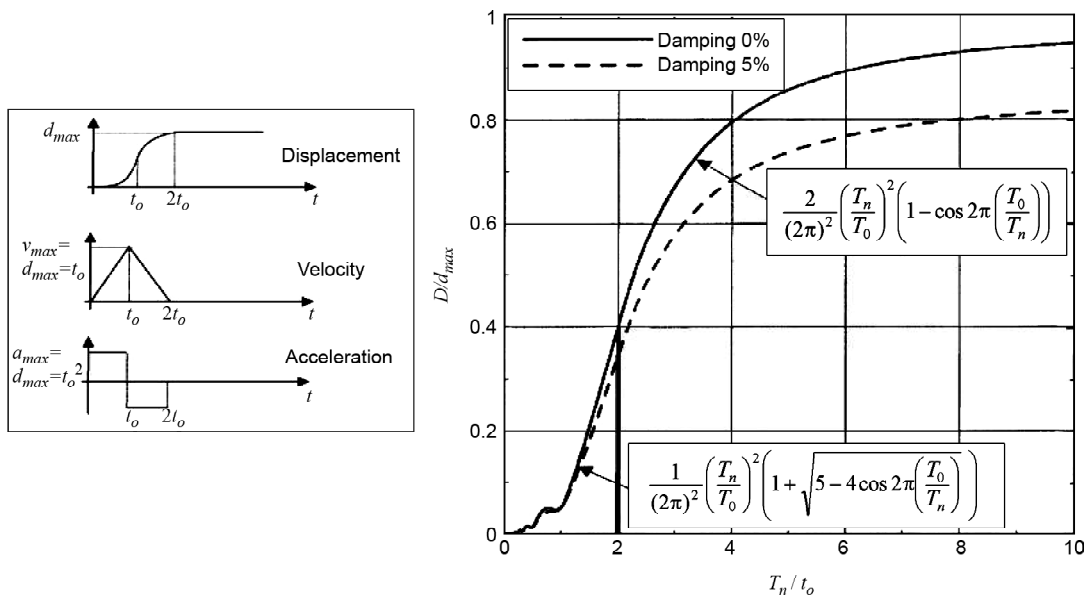

Figure 10. Long-period displacement spectrum of a step pulse [6].
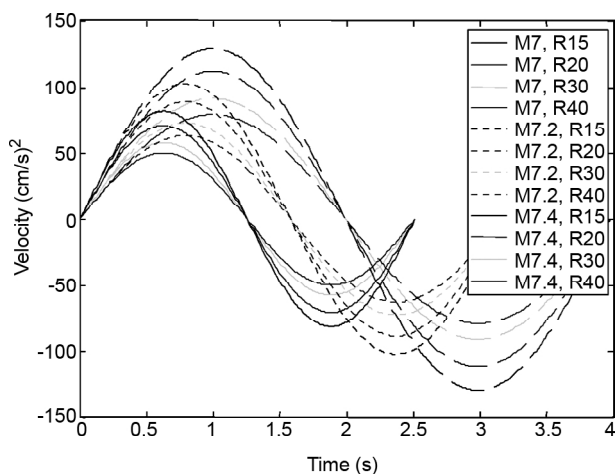

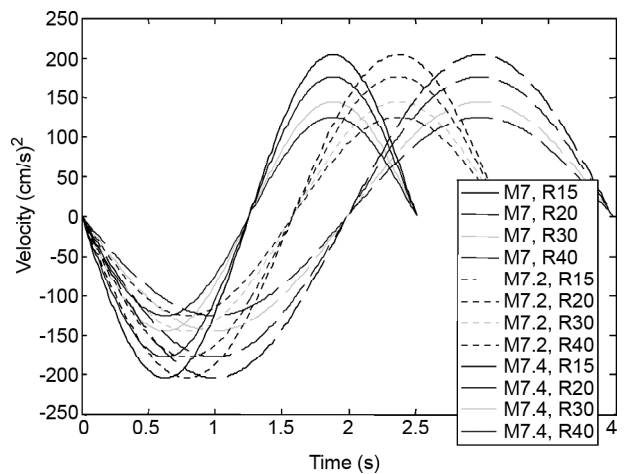**Figure 11.** The form of the velocity pulses derived by Eq. (36).

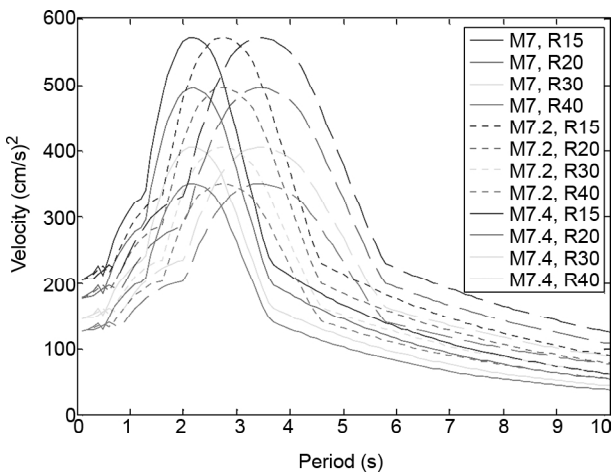**Figure 12.** Corresponding acceleration pulses.

Figure 13. Corresponding acceleration spectra.

6. Probabilistic Hazard Assessment for Spectral Displacement Amplitudes and Hazard Deaggregation

A simple and direct way of capturing the magnitude- and distance-dependence of the spectral displacement ordinates at different damping levels would be to define a series of design spectra with different damping values for *DBD* in future seismic design codes. An example of which is given in Figure (14) for Turkey, where the 5% damped spectral displacement amplitudes at 4*s* are plotted for 2% probabilities of exceedance in 50 years. Please note that these values may not be reliable within 20*km* of the main fault zones since the rupture directivity effects are not incorporated.

Probabilistic seismic-hazard deaggregation involves determining earthquake variables, principally magnitude, distance and values of other random variables defining seismic events that contribute to a selected seismic-hazard level [30]. The deaggregation of seismic hazard is an effective way to identify scenario events that contribute to a selected seismic-hazard level. These scenario earthquakes are to be considered in the definition of the controlling-event response spectrum, time history and/or to select strong-motion records for use in dynamic structural analysis. The ground motion parameter that might be recorded or computed from a record at a specific site (say, the spectral displacement at period *T*, (*SD*(*T*)) from an earthquake with a magnitude (*M*) and distance (*R*) is typically modeled as a lognormal variable. That is, the logarithm of *SD*(*T*), which we denote as *ln*(*SD*(*T*)) has a normal distribution, with mean (*m*) and standard deviation (*s*):

$$ln(SD(T)) = f(M_r, R_r \propto) + \varepsilon\sigma \qquad (37)$$

Here ∝ represents the regression variables *M* and *R* (such as source mechanism and site conditions) and εσ is the error term. Epsilon (ε) is a measure of the deviation of ground motion parameter (*SD*(*T*)) from the predicted median value. Epsilon is defined as the number of standard deviations by which an observed logarithmic spectral displacement differs from the mean logarithmic spectral displacement of a ground-motion prediction (attenuation) equation.

Deaggregation of the hazard for spectral displacement at 10*s* (*SD*(10*s*)), which has been indicated to
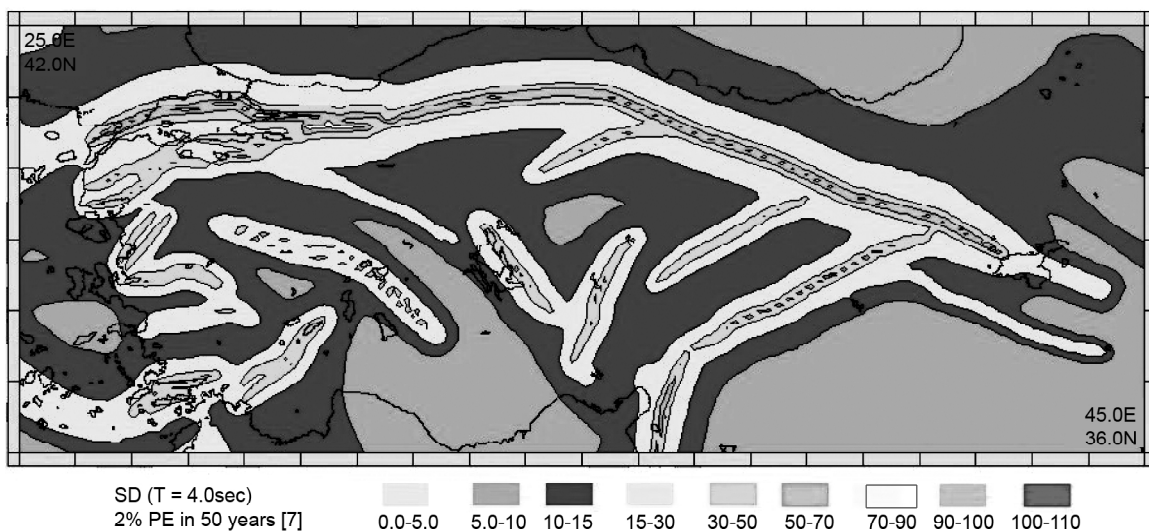

Figure 14. 5% spectral displacement at 4s for 2475 year average return period.

correspond to the plateau level of the displacement spectrum) has been carried out for points located at distances 0, 10, 20, 30, 40 and 50*km* from the Main Marmara Fault at the Asian and European sides of Istanbul. All of the ground motion parameters are associated with *NEHRP* site class *B/C* boundary. These points are illustrated on Figure (15). Tables (1) and (2) provide the hazard deaggregation results for 475 and 2475 years respectively for the points in Asian and European sides.

Although there is some slight variation with respect to distance, it can be assessed that with engineering accuracy, the 475 year average return period $SD(10s)$ can be obtain as median-plus-1.3
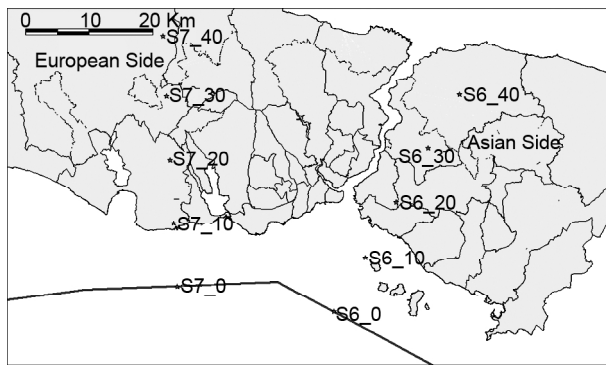

Figure 15. Points at which hazard deaggregation studies were conducted.

standard deviation and the 2475 year average return period $SD(10s)$ can be obtain as median-plus-2.0 standard deviation. For the attenuation relationships we would suggest the *NGA* attenuation relationships [31].

7. Conditional Mean Spectrum and Compatible Ground Motion

Response spectral shape over a period range of significance to structural response has been found to be closely correlated to inelastic structural response and behavior in a number of studies. The period range of significance may include periods shorter and longer than the fundamental structure period respectively because of the higher-mode effects and due to softening during inelastic response. In practice sets of time series are formed to provide a match to a probabilistic response spectrum (equal or uniform hazard spectrum, *UHS*) for design purposes or deterministic scenario earthquake design spectra (again *UHS*), on the basis of hazard deaggregation and appropriate *GMPEs*, can be determined. It should be noted that, the *UHS* is not the response spectrum of ground motion from a single earthquake and as such, has an artificial shape that cannot be physically realized. Since it represents the envelope of the spectra from a multitude of earthquakes, it

Table 1. Deaggregation results for the Asian Side (SD(10 s)).

Station Name		S6_10		S6_20		S6_30		S6_40	
Return Period (Year)		10*km*		20*km*		30*km*		40*km*	
		Mean	Mode	Mean	Mode	Mean	Mode	Mean	Mode
475	M	7.3	7.25	7.3	7.25	7.4	7.25	7.4	7.25
	D	29	11.25	50	21.25	66	31.25	80	41.25
	E	1.3	0.9	1.5	1.1	1.5	1.3	1.5	1.3
2475	M	7.3	7.25	7.4	7.25	7.4	7.25	7.5	7.25
	D	25	11.25	49	21.25	69	31.25	85	41.25
	E	1.9	1.5	2.1	1.9	2.1	1.9	2.1	1.7

Table 2. Deaggregation results for the European Side (SD(10s)).

Station Name		S7_10		S7_20		S7_30		S7_40	
Return Period (Year)		10*km*		20*km*		30*km*		40*km*	
		Mean	Mode	Mean	Mode	Mean	Mode	Mean	Mode
475	M	7.3	7.25	7.4	7.25	7.4	7.25	7.4	7.25
	D	30	11.25	46	21.25	59	33.75	71	43.75
	E	1.4	1.3	1.5	1.3	1.5	0.9	1.4	1.5
2475	M	7.3	7.25	7.4	7.25	7.5	7.25	7.5	7.85
	D	28	11.25	47	21.25	62	76.25	74	81.25
	E	2	1.5	2.1	1.9	2	2.1	2	1.5

M = Magnitude, D = Distance, E = Epsilon

can be overly conservative.

Under such conditions, it would be rational and appropriate to define a spectra (conditional mean spectra) that are conditioned on a spectral value at a given period and the associated ε [32-34]. The resulting target spectrum (Conditional Mean Spectrum-*CMS*) maintains the probabilistic rigor of *PSHA*, so that consistency is achieved between the *PSHA* and the ground motion selection. The conditional mean spectrum furthermore, reflects the lack of perfect correlation between spectral accelerations at different periods, so that if a high spectral acceleration is observed at one period, it is unlikely that it will be observed at other periods.

The conditional mean target spectrum can be constructed by (1) Selecting a target *Sa*(*T*1) value, (2) Computing conditional mean ε values at other periods, given ε(*T*1), (3) Computing *Sa* values at other periods, given the target *M*, *R* and ε's. The steps involved in calculating a conditional mean spectrum are summarized in Figure (16).

The *MATLAB* code prepared by the Baker Research Group can be used to select conditional (structure- and site- specific) ground motions based on the Campbell and Bozorgnia [17] ground-motion model. The target means and covariances are obtained corresponding to a pre-defined target scenario earthquake, and are obtained based on the *CMS* method. The target means and variances can be modified by the user. The function used for the
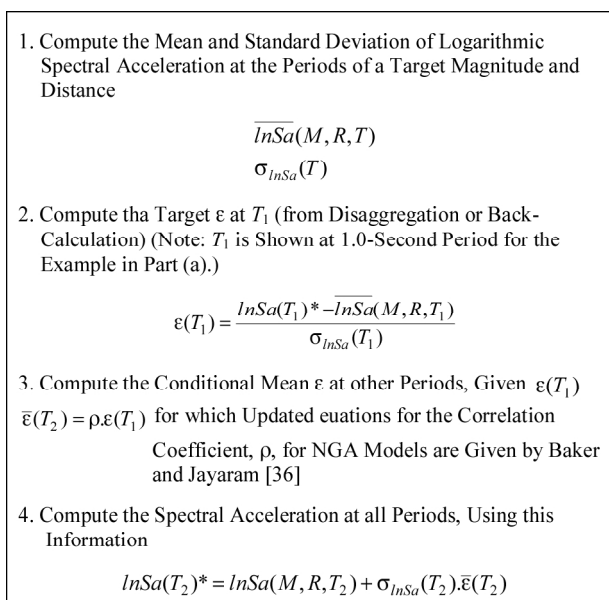
computation of the correlation of epsilons for the *NGA* ground motion models is strictly empirical, fitted over the range the range 0.01*s* to 10*s*. The ground motion selection algorithm can be based on a single arbitrary ground motion component (for two-dimensional structural models), or on the geometric mean of two ground motion components (for three-dimensional structural models), as described in Jayaram et al [36] and Baker [34].

Figure (17) represents the conditional mean spectra at period 6*s* for epsilon (ε) = 0.1; 1.35; and 2.0 and response spectra of ground motions scaled with respect to conditional mean spectrum.
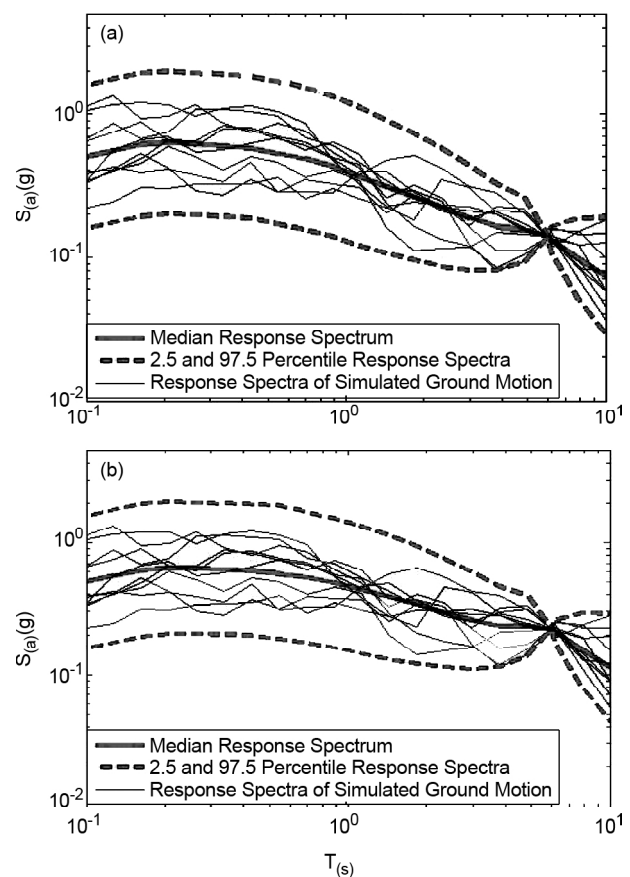

Figure 17. Response spectra of simulated ground motions for (a) epsilon = 1.35 and (b) 2.0.

8. Simulation of Long-Period Ground Motion

Near-fault ground motions are not adequately represented in modern codes. Furthermore, the empirical strong motion database for these conditions is extremely limited and thus the existing attenuation relationships only use poor extrapolations into this underrepresented magnitude-distance space. Although techniques exist for determining response spectra of the ground motion for near fault

---

1. Compute the Mean and Standard Deviation of Logarithmic Spectral Acceleration at the Periods of a Target Magnitude and Distance

$$\overline{lnSa}(M,R,T)$$
$$\sigma_{lnSa}(T)$$

2. Compute tha Target ε at T_1 (from Disaggregation or Back-Calculation) (Note: T_1 is Shown at 1.0-Second Period for the Example in Part (a).)

$$\varepsilon(T_1) = \frac{lnSa(T_1)^* - \overline{lnSa}(M,R,T_1)}{\sigma_{lnSa}(T_1)}$$

3. Compute the Conditional Mean ε at other Periods, Given ε(T_1)

$$\bar{\varepsilon}(T_2) = \rho.\varepsilon(T_1)$$ for which Updated euations for the Correlation Coefficient, ρ, for NGA Models are Given by Baker and Jayaram [36]

4. Compute the Spectral Acceleration at all Periods, Using this Information

$$lnSa(T_2)^* = \overline{lnSa}(M,R,T_2) + \sigma_{lnSa}(T_2).\bar{\varepsilon}(T_2)$$

Figure 16. Steps in calculating conditional mean spectrum, Modified from Baker [35].

conditions, spectral matching techniques cannot build a forward directivity pulse and furthermore the three components of ground motion can not be created with proper phase characteristics (in the period ranges of concern) from a response spectrum.

The primary concern is that the assessment of design basis ground motion for base isolated structures is the rational representation long-period components of the ground motion. Apart from the basin response effects, the main factor that influences the long period ground motion comes from the forward rupture directivity associated with near-fault effects [37].

These conditions necessitate the use of theoretical simulation models. At the periods of concern for base-isolated buildings (i.e. between 2-4*s*) in the near-fault conditions these motions can be assessed for given fault rupture characteristics in a deterministic approach through theoretical simulation models. Such simulations can produce reliable sets of tri-axial ground motion with proper amplitude and phase characteristics in period ranges of concern for the basis-isolated structures. High frequency ground motions can be added to these ground motions using stochastic approaches.

The approach that was utilized for the rational assessment of the design basis ground motion for the seismically isolated systems is elaborated though applications carried out in connection with the newly designed Erzurum Hospital in Turkey. The hospital is located in the southeastern part of the city of Erzurum in eastern Turkey and is intended to remain operational even under the strongest earthquake that it could be exposed. As such a state-of-the-art base isolation technique will be incorporated to ensure such a demanding performance criteria. The earthquake resistant design of base isolated buildings is regulated by several codes with international applications. The earthquake hazard assessment and the definition of the design basis ground motions should conform to these codes.

Today the capability exists to synthesize/simulate earthquake strong motion over the entire frequency range, and for any source-receiver distance of engineering interest. The synthesis/simulation and prediction techniques can properly account for site effects and are valid for sites both near an extended fault/source as well as at far-field.

The Kinematic Modeling Approach involves the prediction of motions from a fault that has specific

dimensions and orientation in a specified geologic setting. As such, this approach more accurately reflects the various wave propagation phenomena and is useful for site-specific simulations. In this Approach the rupture process is modeled by postulating a slip function on a fault plane and then using the Elastodynamic Representation Theorem the ground motion is computed, e.g. [38]. There are several variants of this approach depending on whether the slip function (i.e., the function that describes the evolution of slip on the fault plane) and/ or the Green functions are synthetic or empirical.

9. Conclusions

Although there are several physical models and the associated numerical techniques to simulate ground motions, they do not give consistent results, and their indiscriminate use does not necessarily yield reliable estimates of ground motions for design. The ability to determine motions at longer periods than before has an important application in displacement-based design.

There is a strong need for the development of robust and reliable techniques for the assessment of long-period earthquake ground motions especially for near field conditions. The efforts should address:

- ❖ The principles for modification of design basis spectra in the long-period range (2-10s);
- ❖ Guidelines for time domain simulation of long-period ground motions; and
- ❖ Rules for selecting and scaling ground motion records to address long-period effects.

References

1. IBC (2006). "International Building Code", International Code Council, Virginia, USA.

2. EC-8 (2003). "Design Provisions for Earthquake Resistance of Structures", Publication ENV-2003-2, Comite European de Normalizations, Brussels.

3. Tolis, S. and Faccioli, E. (1999). "Displacement Design Spectra", *Journal of Earthquake Engineering*, **3**, 107-125.

4. Bommer, J.J. and Elnashai, A.S. (1999). "Displacement Spectra for Seismic Design", *Journal of Earthquake Engineering*, **3**(1), 1-32.

5. NEHRP (2003). "2003 NEHRP Recommended Provisions for New Buildings and Other Structures (FEMA 450)", Building Seismic Safety

Council, The National Institute of Building Sciences, USA.

6. Faccioli E., Paolucci, R., and Rey, J. (2004). "Displacement Spectra for Long-Periods", *Earthquake Spectra*, **20**, 347-376.

7. Akkar, S. and Bommer, J.J. (2007). "Empirical Prediction Equations for Peak Ground Velocity Derived from Strong-Motion Records from Europe and the Middle East", Bulletin of the Seismological Society of America, **97**(2), 511-530.

8. Cauzzi,C., Faccioli, E., and Paolucci, R. (2007). "A Reference Model for Prediction of Long-Period Response Spectral Ordinates-Deliverable D2 (Task 1)", Politecnico di Milano.

9. EC-8 (1998). "Design Provisions for Earthquake Resistance of Structure", Eurocode-8, European Committee for Standardization.

10. Priestley, M.J.N., Calvi, G.M., and Kowalsky, M.J. (2007). "Displacement-Based Seismic Design of Structures", IUSS Press, Pavia, Italy, 720.

11. Priestley, M.J.N. (2003). "Myths and Fallacies in Earthquake Engineering", Revisited, IUSS Press, Pavia, Italy.

12. Gregor, N.J. and Bolt, B.A. (1997). "Peak Strong Motion Attenuation Relations for Horizontal and Vertical Ground Displacements", *Journal of Earthquake Engineering*, **1**(2), 275-292.

13. Bommer, J.J., Elnashai, A.S., and Weir, A.G. (2000). "Compatible Acceleration and Displacement Spectra for Seismic Design Codes", *Proc. 12th World Conf. on Earthquake Engineering*, Auckland, New Zealand, New Zealand Society for Earthquake Engineering, Inc., Wellington, New Zealand, Paper No. 207.

14. Tromans, I.J. and Bommer, J.J. (2002). "The Attenuation of Strong-Motion Peaks in Europe", *Proceeding of the 12th European Conference on Earthquake Engineering, London*, 394.

15. Ambraseys, N.N, Simpson, K.A., and Bommer, J.J. (1996). "Prediction of Horizontal Response Spectra in Europe", *Earthquake Engineering and Structural Dynamics*, **25**, 371-400.

16. Gregor, N.J., Silva, W.J., Wong, I.G., and Youngs, R.R. (2002). "Ground-Motion Attenuation Relationship for Cascadia Subduction Zone Megathrust Earthquake Based on a Stochastic Finite-fault Model", Bulletin of the Seismological Society of America, **92**, 1923-1932.

17. Campbell, K.W. and Bozorgnia, Y. (2008). "NGA Ground Motion Model for the Geometric Mean Horizontal Component of PGA, PGV, PGD and 5% damped Linear Elastic Response Spectra for Periods Ranging from 0.01 to 10s", *Earthquake Spectra*, **24**, 139-171.

18. Beresnev, I.A. and Atkinson, G. (1997). "Modeling Finite Fault Radiation from the Tn Spectrum", Bulletin of Seismological Society of America, **87**, 67-84.

19. Erdik, M. and Durukal, E. (2002). "Simulation Modeling of Strong Ground Motion", in Earthquake Engineering Handbook, W-F. Chen and C. Scawthorn, Editors, CRC Press.

20. Beresnev, I.A. (2001). "What We Can and Cannot Learn about Earthquake Sources from the Spectra of Seismic Waves", *Bulletin of Seismological Society of America*, **91**, 397-400.

21. Hanks, T.C. and Kanamori, H. (1979). "A Moment Magnitude Scale", *Journal of Geophysical Research*, **84**(b5), 2348-2350.

22. Somerville, P.G., Smith, N.F., Graves, R.W., and Abrahamson, N.A. (1997). "Modification of Empirical Strong Ground Motion Attenuation Relations to Include the Amplitude and Duration Effects of Rupture Directivity", *Seismological Research Letters*, **68**(1), 199-222.

23. Veletsos, A.S. and Newmark, N.M. (1964). "Response Spectra for Single-Degree-of-Freedom Elastic and Inelastic Systems", Rept. No. RTD-TDR-63-3096, **3**, Air Force Weapons Lab., Albuquerque, N. Mexico.

24. Mavroeidis, G.P. and Papageorgiou, A.S. (2003). "A Mathematical Representation of Near-Fault Ground Motions", Bulletin of the Seismological Society of America, **93**(3), 1099-1131.

25. Somerville, P.G. (2003). "Magnitude Scaling of the Near Fault Rupture Directivity Pulse", Physics of the Earth and Planetary Interiors, **137**, 201-212.

26. Fu, Q. and Menun, C. (2004). "Seismic-Environment-Based Simulation of Near-Fault Ground Motions", *Proceedings of the 13ᵗʰ World Conference on Earthquake Engineering*, Vancouver, Canada, 15.

27. Akkar, S., Sucuoglu, H., and Yakut, A. (2005). "Displacement-Based Fragility Functions for Low- and Mid-Rise Ordinary Concrete Buildings", *Earthquake Spectra*, **21**(4), 901-927.

28. Baker, J.W. (2007). "Quantitative Classification of Near-Fault Ground Motions using Wavelet Analysis", Bulletin of the Seismological Society of America, **97**, 1486-1501.

29. Somerville, G.P. (2004). "Near Fault Directivity Pulse Model: Development and Application in Scenario and Probabilistic Maps of Pulse Parameters in the San Francisco Bay Area", URS Greiner Woodward Clyde.

30. Bazzurro, P. and Cornell, C.A. (1999). "On Disaggregation of Seismic Hazard", Bulletin of Seismological Society of America, **89**(2), 501-520.

31. Earthquake Spectra Issue about NGA (2008). http://peer.berkeley.edu/products/nga_project.html, **24**(1), 1-341.

32. Baker, J.W. and Cornell, C.A. (2008a). "Vector-valued Intensity Measures Incorporating Spectral Shape for Prediction of Structural Response", *Journal of Earthquake Engineering*, **12**(4), 534-554.

33. Baker, J.W. and Jayaram, N. (2008b). "Correlation of Spectral Acceleration Values from NGA Ground Motion Models", *Earthquake Spectra*, **24**(1), 299-317.

34. Baker, J.W. (2011). "Conditional Mean Spectrum: Tool for Ground Motion Selection", *Journal of Structural Engineering*, **137**(3), 322-331, http://dx.doi.org/10.1061/(ASCE)ST.1943-541X.0000215.

35. Baker, J.W. (2006). Breaking the Uniform Hazard Spectrum into Component Events: The Effect of Epsilon on Response Spectra and Structural Response: Preprinted Presentation from 2006 COSMOS Technical Session Entitled "An Evaluation of Methods for the Selection and Scaling of Ground Motion Time series for Building Code and Performance-Based Earthquake Engineering Applications", Sponsored by Consortium of Organizations for Strong-Motion Observation Systems and Pacific Earthquake Engineering Research Center, Berkeley, California, http://www.cosmos-eq.org/presentations/TS2006/6-Baker.pdf

36. Jayaram, N., Lin, T., and Baker, J.W. (2011). "A Computationally Efficient Ground-Motion Selection Algorithm for Matching a Target Response Spectrum Mean and Variance", *Earthquake Spectra*, **27**(3), 797-815.

37. Durukal, E. and Erdik, M. (2006). "Characterization of Strong Ground Motion for the Design of Seismically Isolated Structures for Near-Fault Conditions", *Proceedings of the 4ᵗʰ World Conf. on Structural Control and Monitoring*, International Association for Structural Control and Monitoring, San Diego, California, Paper No. 234.

38. Aki, K. and Richards, P.G. (1980). "Quantitative Seismology", Freeman and Co., New York.